DOI: 10.1002/ejic.200701267

Trigonal-Pyramidal Tetra-Sandwich Complexes as 3D NLOphores

Stefan Steffens,[a] Marc H. Prosenc,[a] Jürgen Heck,*[a] Inge Asselberghs,[b] and Koen Clays[b]

Keywords: Second harmonic generation / Tetranuclear sandwich complexes / 3D NLOphores / X-ray structure determination / Redox properties / Iron / Ruthenium

The Negishi cross-coupling reaction of 1,3,5-trihalobenzene with ferrocenyl- and ruthenocenyllithium, yields the corresponding 1,3,5-trimetallocenylated benzene derivatives in good yield, when 1,3,5-triiodobenzene is used. In a subsequent stacking reaction with the cationic (η^5-cyclopentadienyl)ruthenium(II) and (η^5-pentamethylcyclopentadienyl)ruthenium(II) half-sandwich complexes to the central benzene ring, the trigonal-pyramidal tetra-sandwich complexes (η^5-cyclopentadienyl)(η^6-1,3,5-triferrocenylbenzene)-ruthenium(II) hexafluorophosphate (**4**), (η^5-pentamethylcyclopentadienyl)(η^6-1,3,5-triferrocenylbenzene)ruthenium(II) hexafluorophosphate (**5**) and (η^5-cyclopentadienyl)-(η^6-1,3,5-triruthenocenylbenzene)ruthenium(II) hexafluorophosphate (**6**) are formed. X-ray structure analyses of the complexes **4** and **6** confirm the trigonal-pyramidal architecture composed of four sandwich units. Cyclic voltammetric studies of the ferrocenyl-containing complexes **4** and **5** reveal only one reversible redox couple with a peak separation of $\Delta E_p < 80$ mV, demonstrating a negligible mutual electronic influence of the ferrocenes in all *meta* positions. The positive charge of the central sandwich cation shifts the oxidation potential anodically to +186(5) and +154(5) mV vs. ferrocene/ferrocenium for **4** and **5**, respectively. Based on a charge/NMR shift correlation, the charge flow from the metallocenes to the central sandwich unit can be calculated. Concerning the second harmonic generation (SHG), **4** demonstrates a larger first hyperpolarizability β than the all-ruthenium congener **6** due to the better electron-donating properties of the ferrocene substituents. The structural data, the redox behaviour and the experimentally obtained charge flow from the donor to the acceptor units are in good agreement with the results of corresponding DFT calculations.

Introduction

Organometallic polysandwich complexes are expected to provide very interesting properties with high potential for applications,[1] e.g. in molecular motors,[2] in electron-storage devices,[3] as redox catalysts,[4] and in materials with nonlinear optical properties.[5]

In our research regarding new organometallic structural motifs directed towards second harmonic generation (SHG), we quite extensively studied dipolar "1D" NLOphores, containing sandwich-type complexes as electron-donating and -accepting groups.[6] Another type of compounds, which is prone to SHG, is nonpolar but still lacking a centre of symmetry as a "conditio sine qua non" to demonstrate SHG.[7] Typical representatives are so-called "2D" NLOphores which are realized e.g. in dendritic compounds obeying D_{3h}, C_3 or C_{3v} symmetry.[8] For our research it seems obvious to combine the principles of 1D and 2D NLOphores to construct novel organometallic NLO complexes composed of a 2D NLOphore with threefold symmetry which on top is furnished with a central aromatic unit coordinated to a cationic metal complex acting as an electron-accepting group. Such complexes may be regarded as "3D" NLOphores.

In this article we present first results of the synthesis of such pyramidal dendritic complexes (Figure 1), their spectroscopic and structural properties as well as results of hyper-Rayleigh scattering (HRS) measurements with respect to their first hyperpolarizability β.[9]

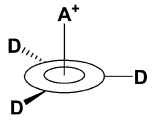

Figure 1. Trigonal-pyramidal NLOphores composed of a dendritically arranged organometallic donor system (D) and a central cationic organometallic acceptor unit (A^+).

Results and Discussion

In order to synthesize the trigonal-pyramidal target complexes, the 1,3,5-trimetallocenylated benzene derivatives **2** and **3** have to be prepared first, whose central benzene ring would then be coordinated to a cationic electron-accepting group. In the literature different routes are described for the

[a] Department Chemie – Anorganische und Angewandte Chemie, Universität Hamburg,
Martin-Luther-King-Platz 6, 20146 Hamburg, Germany
[b] Department of Chemistry, University of Leuven,
Celestijnenlaan 200D, 3001 Leuven, Belgium

synthesis of 1,3,5-triferrocenylated benzene **2**: a Pd-catalyzed Negishi cross-coupling reaction,[10] a transition-metal-catalyzed cyclotrimerization of ethynylferrocene[11] and an acid-catalyzed trimerization of acetylferrocene.[12–14] The best yields without additional isomers and other ferrocenylated benzene derivatives, which had to be separated by chromatography, were reported for the Negishi cross-coupling reaction. In addition, the synthesis of the ruthenocenyl compound **3** has not been reported yet. Therefore, and because of our experience in monolithiation of metallocenes[6,15–17] the Negishi cross-coupling reaction was chosen as the synthetic route to **2** and **3**. The use of ruthenocene in addition to ferrocene as electron-donating metallocenes in this research project was motivated by the observation that ferrocene-containing NLOphores very often show fluorescence due to two-photon absorption in contrast to the ruthenocene congeners.[15–17]

The appropriate metallocene was monolithiated by conducting the method as described.[18] The corresponding zinc compound was generated in situ by adding a thf solution of water-free zinc chloride. The organic halide and the precursor of the catalyst were added. A ^{1}H NMR spectrum of the crude reaction product indicated several compounds, which were purified by column chromatography. As by-products the corresponding metallocenylated halobenzene derivatives could be identified but were not further characterized.

From the result of the reaction described in Scheme 1 it is quite obvious that – as expected – transformations with 1,3,5-triiodobenzene proceed with distinctly higher yields of the desired 1,3,5-trimetallocenylated products **2** and **3** than with the corresponding bromobenzene substrate. Finally, compounds **2** and **3** were subjected to a coordination reaction with $[(C_5R_5)Ru(NCMe)_3]PF_6$[19,20] (Scheme 2) to yield the cationic trigonal-pyramidal NLOphores **4**, **5** and **6** containing four sandwich units.

X-ray Structure Analysis

Suitable crystals of **4** and **6** could be obtained through gas-phase diffusion of diethyl ether into concentrated solutions of **4** and **6** in acetonitrile. Complex **4** crystallizes in the monoclinic space group *C*2/*c* with one molecule of acetonitrile per complex unit, and for **6** the monoclinic space group $P2_1$ was found. Both complexes crystallize in a typical trigonal-pyramidal conformation: the three metallocenyl substituents adopt an all-*cis* conformation, whereas the cationic mixed-sandwich unit $[Ru(\eta^6\text{-arene})(\eta^5\text{-Cp})]^+$ takes the central position in *trans* conformation with respect to the metallocenes (Figures 2 and 3, Table 1). The substituted Cp ligands of the ferrocenyl units in **4** are almost coplanar to the central six-membered ring. The dihedral angles Ru–X–X–Fe between the vectors defined by the centroids X of the Cp ligands of the ferrocenes, of the arene ligand, and the appropriate metal centres vary from 157.5° to 177.3°; the corresponding dihedral angles Ru–X–X–Ru for the all-ruthenium derivative **6** are smaller and take values of 119.5°, –142.7° and 149.0°. The structural details of all sandwich subunits are as expected from those of the unsubstituted metallocenes[21,22] and (η^6-benzene)(η^5-cyclopentadienyl)-ruthenium(II) hexafluorophosphate.[19a,23]

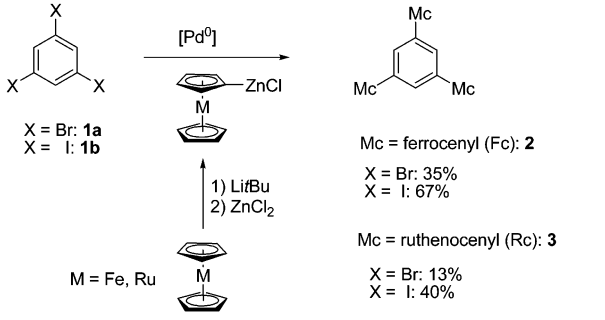

Scheme 1. Negishi cross-coupling reaction to yield trimetallocenylated benzene derivatives.

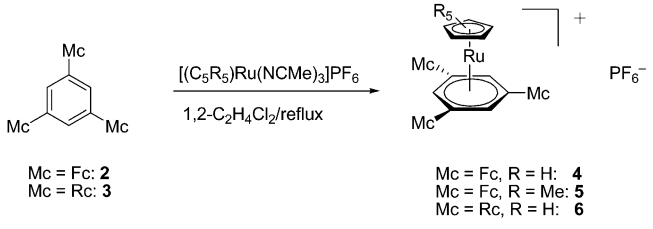

Scheme 2. Synthesis of the trigonal-pyramidal four-sandwich NLOphores **4**, **5** and **6**.

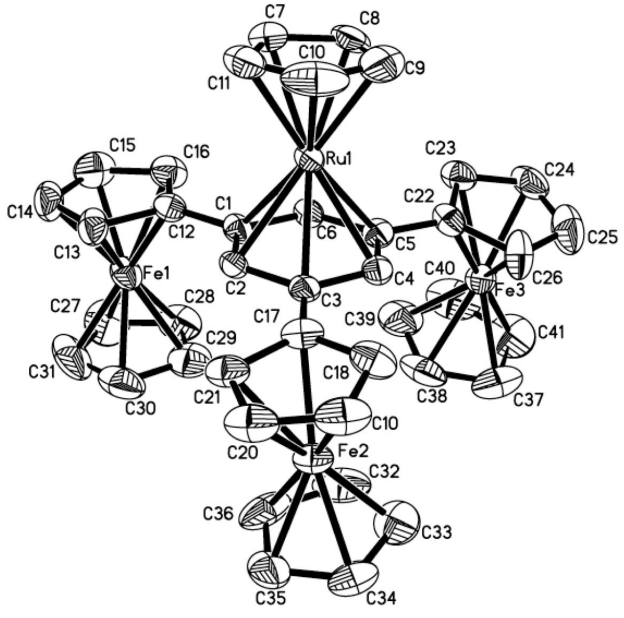

Figure 2. Molecular structure of (η^5-cyclopentadienyl)(η^6-1,3,5-triferrocenylbenzene)ruthenium(II) hexafluorophosphate (**4**) (hydrogen atoms, the solvent molecule acetonitrile and the counterion are omitted for clarity, displacement ellipsoids are drawn at the 50% probability level).

Table 1. Selected inter atomic distances [pm] and dihedral angles [°].

M = Fe, Ru	**4**	**4**-DFT	**6**	**6**-DFT		**4**	**4**-DFT	**6**	**6**-DFT
M–C12	203.5(5)	204.7	215.3(4)	220.0	Ru(1)–C1	222.3(6)	228.3	222.3(4)	228.4
M–C13	204.0(6)	203.8	216.3(4)	219.2	Ru(1)–C2	221.8(6)	222.5	223.2(4)	222.6
M–C14	202.2(6)	205.7	218.4(4)	220.6	Ru(1)–C3	225.9(6)	228.4	222.6(4)	228.6
M–C15	201.6(7)	205.6	219.1(4)	220.5	Ru(1)–C4	222.6(6)	222.6	221.1(4)	222.3
M–C16	203.5(6)	204.0	218.5(4)	219.1	Ru(1)–C5	224.1(6)	228.4	224.4(3)	228.5
M–C27	202.5(7)	205.4	217.6(4)	220.1	Ru(1)–C6	221.0(6)	222.4	220.9(3)	223.1
M–C28	203.7(7)	205.2	219.0(4)	220.3	Ru(1)–C7	216.6(7)	221.2	218.8(4)	222.0
M–C29	203.8(7)	205.7	218.4(4)	221.1	Ru(1)–C8	217.2(6)	221.7	218.2(4)	221.4
M–C30	204.2(7)	206.2	217.5(4)	221.1	Ru(1)–C9	217.1(6)	221.3	218.6(4)	221.5
M–C31	204.0(7)	205.2	217.9(4)	220.5	Ru(1)–C10	216.6(6)	221.5	216.3(4)	221.5
C1–C12	149.3(8)	148.4	148.5(5)	148.1	C3–C17	145.8(8)	147.8	150.8(5)	151.1
	146.4(8)					147.0(8)			
	145.8(8)					149.3(8)			
C5–C22	148.7(8)	146.4	148.5(5)	148.7					
	147.5(8)								
	148.4(8)								
Ru–X–X–M1[a]	A: –167.6	179.3	119.5	175.4	Ru(1)–C11	217.3(7)	221.4	217.2(4)	221.4
	B: –163.7								
	C: 177.3								
Ru–X–X–M2[a]	A: 169.9	177.8	149.0	173.4	Ru–X–X–M3[a]	A: 158.2	172.4	–142.7	179.6
	B: 174.6					B: –171.1			
	C: 173.9					C: –157.5			

[a] The dihedral angles have been obtained by taking the angle between vectors defined by the metal centres and the centroid X of the attached ring.

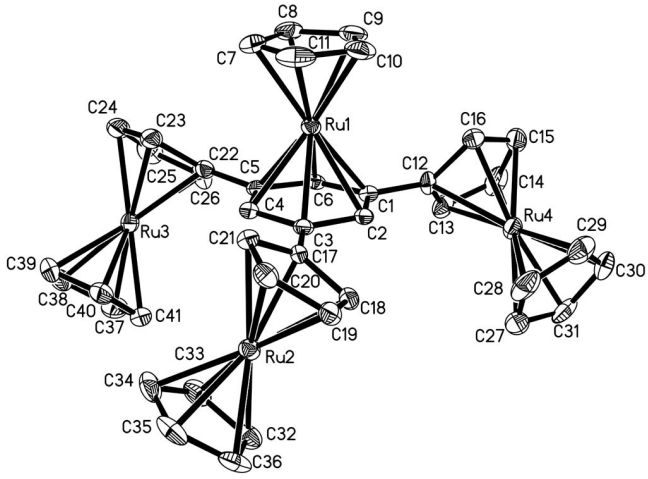

Figure 3. Molecular structure of (η^5-cyclopentadienyl)(η^6-1,3,5-triruthenocenylbenzene)ruthenium(II) hexafluorophosphate (**6**) (hydrogen atoms and the counterion are omitted for clarity, displacement ellipsoids are drawn at the 50% probability level).

Spectroscopic and Electrochemical Properties

UV/Vis spectra of the trigonal-pyramidal four-sandwich complexes **4**–**6** were recorded in CH_2Cl_2 solution (Table 2, Figure 4). The positions of the absorption bands are quite similar to those of ferrocene and ruthenocene[24,25] and the (η^6-benzene)(η^5-cyclopentadienyl)ruthenium(II) cation,[26] but slightly bathochromically shifted and much larger in extinction as mentioned earlier for metallocene-containing donor–acceptor compounds.[16,27] The low-energy absorption bands (λ_{max} = 453 nm for **4**, 448 nm for **5**; for the all-ruthenium complex **6** the low-energy absorption maximum is less separated from the higher-energy band for ruthenocenes than for ferrocenes,[25,27] and may be hidden under the broad absorption band with λ_{max} = 339 nm) are assigned to a donor(metal)–acceptor charge-transfer (D_M–A CT) transition, whereas the higher-energy bands (λ_{max} = 357 nm for **4**, 344 nm for **5** and 339 nm for **6**) are caused by donor(ligand)–acceptor charge-transfer (D_L–A CT) transitions.[27] In accordance to this assignment for **4** and **5**, the D–A CT transitions become more difficult, and the corresponding absorption is hypsochromically shifted when the cationic unit is less electron-withdrawing, caused by permethylation of the cyclopentadienyl ligand in **5** compared to **4** (Table 2). The absorption bands of the electronic excitation at $\lambda \approx$ 335 and 350 nm includes the $^1E_1 \leftarrow {}^1A_1$ transition of the central (η^6-arene)(η^5-cyclopentadienyl)ruthenium unit, which is described as a very weak signal ($\varepsilon <$ 200 $M^{-1}\,cm^{-1}$).[26]

Table 2. UV/Vis spectroscopic and cyclic voltammetry data of the tetranuclear sandwich complexes **4**–**6** and first hyperpolarizabilities of **4** and **6** obtained by HRS measurements with a femtosecond laser (λ = 800 nm).

D/A	λ_{max}[a,b] (ε)[c]	λ_{max}[a,b] (ε)[c]	$E_{1/2}$[d,e]	ΔE_p[f]	β_{800}[h]	β_o[h,i]
4 Fc/RuCp	357 (6500)	453 (2800)	0.186	0.074	46.7	7.6
5 Fc/RuCp*	344 (5400)	448 (1200)	0.154	0.076	n.d.[g]	
6 Rc/RuCp	339 (9700)	not resolved	n.d.[g]		14.5	3.4

[a] Measured in CH_2Cl_2. [b] In nm. [c] In $M^{-1}\,cm^{-1}$. [d] Obtained from CH_2Cl_2 solutions at room temperature, 0.4 M [nBu$_4$N][ClO$_4$] as supporting electrolyte. Ag/AgCl as standard electrode referred vs. $E_{1/2}$(ferrocene/ferrocenium) = 0 V, scan rate: 200 mV/s. [e] Potentials $E \pm 0.005$ V. [f] $\Delta E_p = |E_{pc} - E_{pa}|$. [g] n.d. = not determined. [h] In 10^{-30} esu. [i] Calculated from $\beta_o = \beta_{800}[(1 - 4\lambda_{max}^2/\lambda^2)\text{-}(1 - \lambda_{max}^2/\lambda^2)]$.[35]

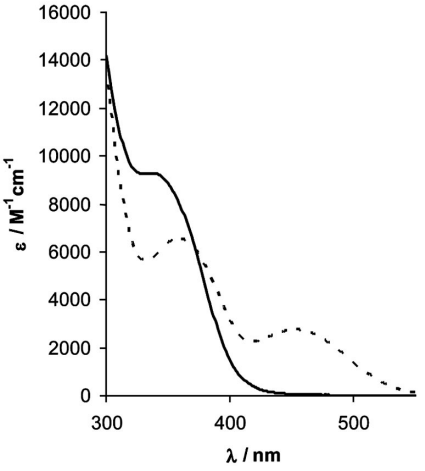

Figure 4. UV/Vis spectra of the trigonal-pyramidal tetra-sandwich complexes **4** (dotted line) and **6** (solid line) (CH_2Cl_2 solutions).

Cyclic voltammetric studies were performed on the ferrocene-containing tetranuclear complexes **4** and **5**. As very recently demonstrated,[28] the 1,3,5-triferrocenylated benzene derivative **2** reveals one single electrochemically reversible redox couple, despite three redox-active ferrocene units, reflecting only a negligible interaction between the ferrocenyl substituents in the all-*meta* positions. Comparable redox behaviour is observed for the cationic tetra-sandwich complexes **4** and **5** with the exception of the oxidation potential (Figure 5). It is anodically shifted to +0.186(5) V for **4** and +0.154(5) V for **5** with respect to ferrocene (Table 2), whereas that of the benzene derivative **2** is cathodically shifted to –0.02 V with respect to ferrocene.[28] The negligible electronic interaction between the ferrocene units in **4** and **5** is also confirmed by a small peak separation of $\Delta E_p \approx 0.075(5)$ V (Table 2). The redox behaviour of the all-*meta*-triferrocenylbenzene derivatives **4** and **5** contrasts the result of *meta*-phenylene-bridged bis(ferrocene) derivatives, where a separation of 60 mV was found between a first and second oxidation.[29]

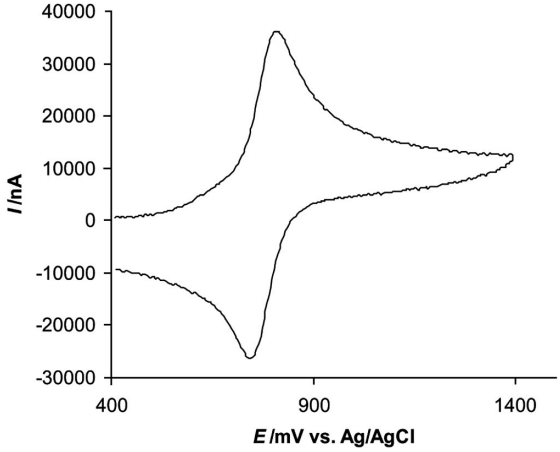

Figure 5. Representative cyclic voltammogram of complex **4**.

A comparison of the oxidation potential indicates the electron-withdrawing character of the central cationic sandwich complex, which is stronger for **4** than for **5** due to the positive inductive effect of the permethylation of the Cp* ligand in **5**.

The electron-withdrawing ability of the cationic sandwich unit can also be substantiated by ^{1}H NMR spectroscopy. For $[(\eta^5\text{-}C_5H_5)Ru(\eta^n\text{-}C_nH_n)]^{m+}$ ($n = 5$, $m = 0$; $n = 6$, $m = 1$; $n = 7$, $m = 2$) sandwich complexes we recently found a linear dependence between the ^{1}H NMR shift of the Cp signal and the charge of the sandwich complex.[17] The relationship enables the calculation of the actual charge for an Ru sandwich entity in donor–acceptor compounds containing $(\eta^5\text{-}C_5H_5)Ru$ units if the proton shift of the Cp signal is known. The singlet of the unsubstituted cyclopentadienyl ligand of the metallocene donor in **6** and the corresponding Cp ligand of the cationic sandwich unit in **4** and **6** are taken as the monitoring signals.

From the shifts of the CpRu units of the donor and the acceptor complexes (Table 3) the corresponding charges of the ruthenocenyl substituents and the CpRu(arene) cation can be calculated taking the empirically found linear correlation into account: $\delta(Cp) = 0.91 \times$ (charge of the CpRu sandwich complex) + 4.55 (Table 3).[17] For **6** the beneficial situation is given that the decrease of charge on the electron-accepting sandwich has to go along with an increase of charge on the ruthenocene donors and thus with a corresponding low-field shift of the Cp resonance signal of the ruthenocenyl donor. The experimental data in Table 3 fulfil this expectation: three times a charge +0.10 for three metallocene units corresponds quite well to a charge reduction to +0.69 on the acceptor sandwich cation. In addition, it is confirmed that a ferrocenyl substituent is a better electron donor than the ruthenium congener: three ferrocenyl substituents in **4** reduce the positive charge on the acceptor complex by about 50%, whereas for **6** the reduction of the positive charge amounts to 30%.

Table 3. ^{1}H NMR shifts of the CpRu unit of the metallocene donor in **6** and of the cationic CpRu unit of the acceptor in **4** and **6**, respectively, and the charge of it, calculated by NMR experiments[a] and by DFT.

	δ(CpRu) donor	Calcd. charge (NMR)	δ(CpRu) acceptor	Calcd. charge (NMR)	Calcd. charge (DFT)
4	–		5.00	0.49	0.51
6	4.64	0.10	5.18	0.69	0.61

[a] Calculated with the empirically found linear correlation $\delta(Cp) = 0.91 \times$(charge of the CpRu sandwich complex) + 4.55.[17]

MO Calculations

For comparison with experimental charge data, calculations on the density functional theory level have been performed on the complex cations **4** and **6**. Geometry optimizations revealed bonding parameters listed in Table 1, which are in good agreement with those experimentally obtained except the expected elongation of the metal–C_5 ring

distances. The calculated charges accumulated on the central sandwich unit are listed in Table 3 and indicate a good conformity with the experimentally determined charges, which were obtained by means of ^{1}H NMR spectroscopy. From our calculations it can be concluded that interaction between the metal centres is slightly more pronounced in complex cation **4** than in cation **6**. This is supported by the calculated and experimentally obtained carbon–carbon bond lengths between the C_6 ring and the C_5 rings, which on the whole are slightly shorter for cation **4** than for cation **6**. In addition, the larger dihedral angles Ru–X–X–M for **4** (M = Fe) than for **6** (M = Ru) indicate the higher degree of conjugation in **4** between the metallocene and Ru moiety.

The analysis of the frontier molecular orbital structure of **4** revealed two sets of nearly threefold degenerate occupied orbitals (HOMOs) in a very close energetic range (0.05 eV, Figure 6). These orbitals have main contributions of Fe d_{xy} and $d_{x^2-y^2}$ atomic orbitals as expected from calculations of ferrocene itself. The nearly threefold degeneracy of the HOMOs for **4** is in good harmony with the single electrochemical oxidation step found in the cyclic voltammetry study. However, the low resonance (mixing) of the nearly degenerate orbitals (states) in ground and excited states prohibits a large hyperpolarizability due to the three-state-model.[7]

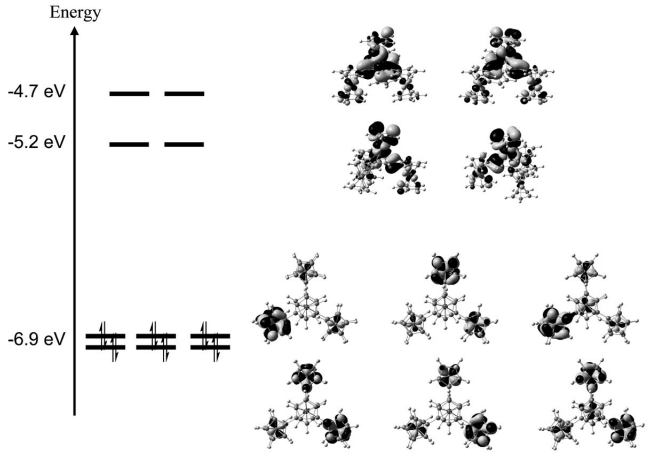

Figure 6. Valence molecular orbital diagram of cation **4**.

NLO Measurements

$MeNO_2$ solutions of the tetranuclear complexes **4** and **6** were subjected to hyper-Rayleigh scattering (HRS) measurements at λ = 1064 nm.[30] These measurements demonstrate a weak SHG effect, which, however, was too weak to calculate the first hyperpolarizability. Therefore, HRS studies were performed with a femtosecond laser source working at 800 nm. This wavelength ensures a larger degree of resonance enhancement for the signal, while the femtosecond pulses offer the temporal resolution to differentiate between potential fluorescence and nonlinear scattering.[31–33] The resulting values for the first hyperpolarizability are given in Table 2.

The HRS signal has been analyzed towards a single hyperpolarizability value, which does not correspond to a specific, symmetry-dependent, hyperpolarizability tensor component. Therefore, the reported values do not assume a specific symmetry for the complexes, but comparison of the hyperpolarizability between the complexes should be possible in view of the very similar molecular structure. The dynamic values, denoted as β_{800}, are strongly resonantly enhanced, because of the proximity of the maximum of absorption to the second-harmonic wavelength. The static values, denoted as β_o, are corrected for this enhancement according to the two-level model.[34] The validity of this simple model, which was developed for nitroanilines, may be questioned for this study of complexes. However, the relative trend in the result remains the same (higher hyperpolarizability for the complex **4** than for complex **6**). The difference in absolute values is more pronounced, because of the stronger resonance effect for complex **4**, due to the proximity of the absorption band (453 nm) to the second harmonic of the laser wavelength.

Concerning the SHG, **4** demonstrates a larger static first hyperpolarizability β_o than the all-ruthenium congener **6** due to the better electron-donating properties of the ferrocene derivative and the resulting larger degree of effective non-centrosymmetry in the structure of the complex. This is a consequence of the substitution of the ruthenocene in the latter and by the ferrocene in the former complex, and corresponds nicely with the observed linear optical properties (the charge-transfer band at longer wavelengths for **4** than for **6**).

Conclusions

Three novel dendritic multi-sandwich complexes (**4**, **5** and **6**) have been synthesized and structurally characterized (**4** and **6**), which are composed of three metallocene units as electron-donating substituents in 1,3,5-position of a benzene ligand being a part of a central cationic sandwich moiety as an electron-accepting unit. This kind of complexes may be regarded as polar 3D NLOphores, whose donor–acceptor interaction is demonstrated (i) by the increase of the intensity of the absorption bands in electron-excitation spectra compared to the corresponding archetype sandwich compounds and their bathochromic shift, (ii) by the anodic shift of the oxidation potential of the ferrocenyl substituents in **4** and **5** compared to those of ferrocene and the neutral 1,3,5-triferrocenylated benzene in cyclic voltammetric studies, (iii) by the charge flow from the central cationic sandwich complex to the metallocene units as indicated by ^{1}H NMR shifts of the unsubstituted Cp ligands of the CpRu entities in **4** and **6** and in addition confirmed by DFT calculations, and finally (iv) by the determination of the first hyperpolarizability β of **4** and **6** through HRS measurements. As expected, the SHG effect for the ferrocenyl-substituted derivative **4** is larger than for the all-ruthenium congener **6**. However, the SHG effect is rather small, due

to the small polarization length of the NLOphores. Therefore, the synthesis of related dendritic complexes displaying a longer conjugation length is under study.

Experimental Section

General: Manipulations were carried out under dry nitrogen using standard Schlenk techniques. All solvents were saturated with nitrogen. Diethyl ether (Et_2O), tetrahydrofuran (thf), *n*-hexane, *n*-pentane and toluene were freshly distilled from the appropriate alkali metal or metal alloy. 1,2-Dichloroethane ($1,2\text{-}C_2H_4Cl_2$) and nitromethane ($MeNO_2$) were dried with calcium hydride. NMR: Varian Gemini 200 BB; Bruker AM 360; measured at 293 K; chemical shifts relative to TMS. UV/Vis: Perkin–Elmer model 554. IR: KBr pellets; FT-IR, Perkin–Elmer model 325. MS: Finnigan MAT 311 A (EI-MS). HRMS: VG 70-250 S mass spectrometer, resolution 5000, xenon-FAB. Elemental analyses: CHN-O-Rapid, Fa. Heraeus, Zentrale Elementanalytik, Department Chemie, University of Hamburg. 1,3,5-Tribromobenzene, ferrocene and ruthenocene were purchased, 1,3,5-triiodobenzene,[36] tris(acetonitrile)(η^5-cyclopentadienyl)ruthenium(II) hexafluorophosphate,[19] tris(acetonitrile)(η^5-pentamethylcyclopentadienyl)ruthenium(II) hexafluorophosphate,[20] monolithioferrocene and monolithioruthenocene[18] were prepared according to literature procedures.

General Procedure for the Negishi Cross-Coupling Reaction of 1,3,5-Trihalobenzene Towards 1,3,5-Trimetallocenylbenzene: $ZnCl_2(thf)_{1.5}$ was added to a suspension of metallocenyllithium in THF at 0 °C. After 1 h of stirring at room temperature, a thf solution of 1,3,5-trihalobenzene and $PdCl_2(PPh_3)_2$ was added. The reaction mixture was stirred at room temperature for 3 h and hydrolyzed by adding 2 M hydrochloric acid. The organic layer was washed three times with an aqueous saturated $NaHCO_3$ solution. The aqueous layer was washed once with dichloromethane, and the combined organic layers were dried with magnesium sulfate. The organic layer was concentrated to dryness, and the residue was purified by column chromatography (Al_2O_3/5% H_2O) with different solvents. The first two fractions were obtained with petroleum ether (boiling range 60–70 °C) containing the metallocene and the 1,3-dihalo-5-metallocenylbenzene. The third fraction was 1-halo-3,5-dimetallocenylbenzene and was eluted with petroleum ether (boiling range 60–70 °C)/toluene (1:1). Finally, the desired 1,3,5-trimetallocenylbenzene was eluted with pure toluene.

Cross-Coupling with 1,3,5-Tribromobenzene and Ferrocenyl Nucleophiles: Used quantities: ferrocenyllithium (4.32 g, 22.5 mmol) in thf (70 mL), $ZnCl_2(thf)_{1.5}$ (10.75 g, 45 mmol), 1,3,5-tribromobenzene (2.36 g, 7.5 mmol) in thf (6 mL) and $PdCl_2(PPh_3)_2$ (527 mg, 0.75 mmol) in thf (6 mL). Yield of **2**: 633 g (35%) of orange crystals. ^{1}H NMR (200 MHz, $CDCl_3$, TMS, 293 K): δ = 7.43 (s, 3 H, C_6H_3), 4.73 (pseudo-t, J = 1.8 Hz, 6 H, C_5H_4), 4.37 (pseudo-t, J = 1.8 Hz, 6 H, C_5H_4), 4.10 (s, 15 H, C_5H_5) ppm. ^{13}C NMR (50 MHz, $CDCl_3$, TMS, 293 K): δ = 139.25 (C_6H_3), 122.10 (C_6H_3), 85.85 (C_5H_4), 69.95 (C_5H_5), 69.16 (C_5H_4), 66.96 (C_5H_4) ppm. IR (KBr): $\tilde{\nu}$ = 3090, 1594, 1562, 1411, 1385, 1105, 1036, 1001, 922, 820, 730, 692 cm^{-1}. UV/Vis (thf): λ_{max} (ε) = 284 (30703), 451 (1281 M^{-1}cm^{-1}) nm. MS (EI): *m*/*z* (%) = 630 (100) [M^+], 509 (3) [$M^+ - C_5H_5Fe$], 388 (3) [$M^+ - C_{10}H_{10}Fe_2$], 265 (3) [$C_{21}H_{15}^+$].

Cross-Coupling with 1,3,5-Tribromobenzene and Ruthenocenyl Nucleophiles: Used quantities: ruthenocenyllithium (4.32 g, 22.5 mmol), $ZnCl_2(thf)_{1.5}$ (10.75 g, 45 mmol), 1,3,5-tribromobenzene (2.36 g, 7.5 mmol) in thf (6 mL) und $PdCl_2(PPh_3)_2$ (527 mg, 0.75 mmol) in thf (6 mL). Yield of **3**: 169 mg (13%) of pale yellow crystals. ^{1}H NMR (200 MHz, $CDCl_3$, TMS, 293 K): δ = 7.20 (s, 3 H, C_6H_3), 5.00 (pseudo-t, J = 1.8 Hz, 6 H, C_5H_4), 4.67 (pseudo-t, J = 1.8 Hz, 6 H, C_5H_4), 4.50 (s, 15 H, C_5H_5) ppm. ^{13}C NMR (100 MHz, $CDCl_3$, TMS, 293 K): δ = 140.7 (C_6H_3), 127.3 (C_6H_3), 88.9 (C_5H_4), 71.9 (C_5H_5), 71.6 (C_5H_4), 69.8 (C_5H_4) ppm. IR (KBr): $\tilde{\nu}$ = 3094, 2924, 253, 1598, 1463, 1426, 1384, 1101, 1032, 955, 922, 867, 820, 757 cm^{-1}. UV/Vis (thf): λ_{max} (ε) = 318 (1072 M^{-1}cm^{-1}) nm. MS (EI): *m*/*z* (%) = 766 (100) [M^+]. $C_{36}H_{30}Ru_3$ (765.84): calcd. C 56.46, H 3.95; found C 56.21, H 3.98.

Cross-Coupling with 1,3,5-Triiodobenzene: Used quantities: ferrocenyllithium (160 mg, 0.84 mmol) in thf (10 mL), $ZnCl_2(thf)_{1.5}$ (400 mg, 1.68 mmol), 1,3,5-triiodobenzene (97 mg, 0.24 mmol) in thf (0.5 mL) und $PdCl_2(PPh_3)_2$ (14.7 mg, 0.02 mmol) in thf (6 mL). Yield of **2**: 89 mg (67%). Used quantities: ruthenocenyllithium (1.31 g, 5.44 mmol), $ZnCl_2(thf)_{1.5}$ (2.60 g, 11 mmol), 1,3,5-triiodobenzene (780 mg, 1.7 mmol) in thf (3 mL) and $PdCl_2(PPh_3)_2$ (113 mg, 0.16 mmol) in thf (3 mL). Yield of **3**: 522 mg (40%) pale yellow crystalline material.

General Procedure for the Synthesis of the Monocationic 1,3,5-Trimetallocenylbenzene Complexes 4, 5 and 6: A solution of tris(acetonitrile)(η^5-cyclopentadienyl)ruthenium(II) hexafluorophosphate and tris(acetonitrile)(η^5-pentamethylcyclopentadienyl)ruthenium(II) hexafluorophosphate, respectively, in 1,2-dichloroethane and the appropriate 1,3,5-trimetallocenylbenzene was stirred under reflux overnight. The reaction mixture was concentrated to dryness. The residue was extracted with toluene/hexane (1:1), and the remaining solid material was recrystallized from dichloromethane/diethyl ether.

(η^5-Cyclopentadienyl)(η^6-1,3,5-triferrocenylbenzene)ruthenium(II) Hexafluorophosphate (4): Used quantities: tris(acetonitrile)(η^5-cyclopentadienyl)ruthenium(II) hexafluorophosphate (347 mg, 0.80 mmol), 1,2-dichloroethane (15 mL), 1,3,5-triferrocenylbenzene (**6**) (300 mg, 0.48 mmol). Yield of **4**: 43 mg (9.5%) of orange crystals. ^{1}H NMR (200 MHz, CD_2Cl_2, TMS, 293 K): δ = 6.05 (s, 3 H, C_6H_3), 5.01 (pseudo-t, J = 2.0 Hz, 6 H, C_5H_4), 5.03 (s, 5 H, RuC_5H_5), 4.82 (pseudo-t, J = 2.0 Hz, 6 H, C_5H_4) 4.60 (s, 15 H, C_5H_5) ppm; (200 MHz, CD_3NO_2, TMS, 293 K): δ = 6.74 (s, 3 H, C_6H_3), 5.00 [s, 5 H, (arene)Ru(C_5H_5)], 4.99 (pseudo-t, J = 2.0 Hz, 6 H, C_5H_4), 4.61 (pseudo-t, J = 2.0 Hz, 6 H, C_5H_4), 4.32 (s, 15 H, C_5H_5) ppm. ^{13}C NMR (50 MHz, CD_2Cl_2, TMS, 293 K): δ = 102.8 (C_q, C_6H_3), 80.9 [(arene)Ru(C_5H_5)], 78.2 (C_6H_3), 77.3 (C_q, C_5H_4), 70.6 (C_5H_4), 69.6 (C_5H_5), 66.9 (C_5H_4) ppm. IR (KBr): $\tilde{\nu}$ = 3093, 2922, 2853, 1542, 1489, 1455, 1414, 1383, 1322, 1255, 1106, 1040, 1002, 863, 727, 693, 674, 557, 491, 460, 426 cm^{-1}. UV/Vis (CH_2Cl_2): λ_{max} (ε) = 357 (6525), 453 (2769 M^{-1}cm^{-1}) nm. MS (FAB): *m*/*z* (%) = 797 (100) [M^+], 676 (33) [$M - FeC_5H_5^+$]. $C_{41}H_{35}F_6Fe_3RuP{\cdot}0.5H_2O$ (950.31): C 51.82, H 3.82; found C 51.69, H 4.20. HRMS (Xe FAB, matrix *m*-nitrobenzyl alcohol): calcd.796.9848; found 796.9850.

(η^5-Pentamethylcyclopentadienyl)(η^6-1,3,5-triferrocenylbenzene)-ruthenium(II) Hexafluorophosphate (5): Used quantities: tris(acetonitrile)(η^5-pentamethylcyclopentadienyl)ruthenium(II) hexafluorophosphate (350 mg, 0.68 mmol), 1,2-dichloroethane (15 mL), 1,3,5-triferrocenylbenzene (**6**) (285 mg, 0.45 mmol). Yield of **5**: 96 mg (22%) orange crystals. ^{1}H NMR (400 MHz, [D$_6$]acetone, TMS, 293 K): δ = 6.38 (s, 3 H, C_6H_3), 5.14 (pseudo-t, J = 2.0 Hz, 6 H, C_5H_4), 4.50 (pseudo-t, J = 2.0 Hz, 6 H, C_5H_4) 4.15 (s, 15 H, C_5H_5), 1.30 (s, 15 H, CH_3) ppm; (400 MHz, CD_3NO_2, TMS, 293 K): δ = 6.23 (s, 3 H, C_6H_3), 5.02 (pseudo-t, J = 2.0 Hz, 6 H, C_5H_4), 4.67 (pseudo-t, J = 2.0 Hz, 6 H, C_5H_4) 4.32 (s, 15 H, C_5H_5), 1.46 (s, 15 H, CH_3) ppm. ^{13}C NMR (100 MHz, [D$_6$]acetone, TMS, 293 K): δ = 104.3 (C_q, C_6H_3), 95.9 (C_5Me_5), 80.6 (C_6H_3), 78.7 (C_q,

C_5H_4), 72.6 (C_5H_4), 71.7 (C_5H_5), 68.8 (C_5H_4), 10.3 (C_5Me_5) ppm; (100 MHz, CD_3NO_2, TMS, 293 K): δ = 102.5 (C_q, C_6H_3), 94.7 (C_5Me_5), 78.9 (C_6H_3), 77.1 (C_q, C_5H_4), 71.1 (C_5H_4), 70.2 (C_5H_5), 66.9 (C_5H_4), 8.3 (C_5Me_5) ppm. IR (KBr): $\tilde{\nu}$ = 3431, 3090, 2920, 2854, 1653, 1544, 1473, 1453, 1410, 1383, 1256, 1157, 1108, 1040, 1001, 838, 729, 692, 476 cm^{-1}. UV/Vis (CH_2Cl_2): λ_{max} (ε) = 344 (5440), 448 (1180 $M^{-1}cm^{-1}$) nm. MS (FAB): *m/z* (%) = 867 (65) [M^+], 745 (12) [M – $FeC_5H_5^+$]. $C_{46}H_{45}Fe_3RuPF_6 \cdot C_2H_4Cl_2$ (1110.40): calcd. C 51.92, H 4.45; found C 51.94, H 4.94.

(η^5-Cyclopentadienyl)(η^6-1,3,5-triruthenocenylbenzene)ruthenium(II) Hexafluorophosphate (6): Used quantities: tris(acetonitrile)(η^5-cyclopentadienyl)ruthenium(II) hexafluorophosphate (282 mg, 0.65 mmol), 1,2-dichloroethane (10 mL), 1,3,5-triruthenocenylbenzene (**3**) (300 mg, 0.39 mmol). Yield of **6**: 75 mg (20.5%) of light yellow crystals. ^{1}H NMR (400 MHz, CD_3CN, TMS, 293 K): δ = 6.10 (s, 3 H, C_6H_3), 5.33 [s, 5 H, (arene)Ru(C_5H_5)], 4.85 (pseudo-t, *J* = 2.0 Hz, 6 H, C_5H_4), 4.60 (pseudo-t, *J* = 2.0 Hz, 6 H, C_5H_4) 4.27 (s, 15 H, C_5H_5) ppm; (400 MHz, CD_3NO_2, TMS, 293 K): δ = 6.52 (s, 3 H, C_6H_3), 5.26 (pseudo-t, *J* = 2.0 Hz, 6 H, C_5H_4), 5.18 [s, 5 H, (arene)Ru(C_5H_5)], 4.86 (pseudo-t, *J* = 2.0 Hz, 6 H, C_5H_4) 4.64 (s, 15 H, C_5H_5) ppm. ^{13}C NMR (100 MHz, CD_2Cl_2, TMS, 293 K): δ = 101.5 (C_q, C_6H_3), 82.5 (C_q, C_5H_4), 81.0 [(arene)-Ru(C_5H_5)], 80.3 (C_6H_3), 71.8 (C_5H_4), 71.7 (C_5H_5), 69.6 (C_5H_4) ppm. IR (KBr): $\tilde{\nu}$ = 3096, 1626, 1541, 1492, 1455, 1415, 1382, 1317, 1252, 1101, 1058, 1026, 999, 836, 724, 692, 557, 434 cm^{-1}. UV/Vis (CH_2Cl_2): λ_{max} (ε) = 344 (930 $M^{-1}cm^{-1}$) nm. MS (FAB): *m/z* (%) = 933 (15) [M^+]. $C_{41}H_{35}Ru_4PF_6 \cdot 2C_2H_4Cl_2$ (1274.89): calcd. C 42.40, H 3.40; found: C 42.23, H 3.44.

Computational Details: For all calculations on the density functional theory level, the Program RIDFT was used.[37] Energies and geometries were developed on the nonlocal level of theory. For geometry optimization the energies were corrected for nonlocal exchange according to Becke[38] and for nonlocal correlation according to Perdew (BP-86).[39] The SVP-split valence base set was used for C and H atoms.[40,41] For Fe and Ru we used an effective core potential base set (ECP-28-mwb) with an SV functions for the valence region and an additional d-polarization function.[42] For the J_{ij} term approximation an additional auxiliary base set was used.[37,42]

X-ray Structure Determination: Crystals of compounds **4** and **6** suitable for an X-ray structure determination were obtained by gas-phase diffusion of Et_2O into a CH_2Cl_2 solution of the complex at room temperature. The data of **6** were collected with a four-circle diffractometer Hilger and Watts and data of complex **4** were collected with a Bruker Smart-APEX three-circle diffractometer, Mo-K_α, λ = 71.073 pm at 153 K (Table 4). The intensities of data for complex **6** were merged prior solution and refinement by using the Xprep program included in the SHELX suit of programs. The structures were solved by direct methods (SHELXS-86),[43a] and the refinement on F^2 was carried out by full-matrix least-square techniques (SHELXL-97).[43b] All non-hydrogen atoms were refined with anisotropic thermal parameters. The hydrogen atoms were refined with a fixed isotropic thermal parameter related by a factor of 1.2 to the value of the equivalent isotropic parameter of their carrier atom. Weights were optimized in the final refinement cycles. For the structure of complex **4** co-crystallized acetonitrile and water molecules were found and refined. Some of the positions of the solvent molecules were not fully occupied due to slow evaporation of solvent molecules. A residual electron density of 2.4 e/Å^3 at a special position (0.25,0.25,0) could be attributed to a water molecule which is in accord with elemental analysis. CCDC-

Table 4. Crystallographic data of **4** and **6**.

	4	**6**
Empirical formula	$C_{41}H_{35}F_6Fe_3PRu \cdot 0.82CH_3CN \cdot 0.17H_2O$	$C_{41}H_{35}F_6PRu_4$
Formula mass	977.28	1076.97
T [K]	153(2)	153(2)
λ [pm]	71.073	71.073
Crystal system	monoclinic	monoclinic
Space group	*C*2/*c*	$P2_1/n$
Unit cell data		
a [pm]	3163.28(13)	1668.37(8)
b [pm]	1870.43(8)	1066.21(5)
c [pm]	4009.20(17)	2052.54(10)
β [°]	94.7890(10)	111.454(1)
V [10^6 pm^3]	23638.4(17)	3398.1(3)
Z	24	4
$\rho_{calcd.}$ [g cm^{-3}]]	1.522	2.105
Absorption coefficient μ [mm^{-1}]	1.539	1.857
F(000)	11925	2104
Crystal size [mm]	0.07 × 0.29 × 0.53	0.20 × 0.10 × 0.05
θ range [°]	1.66–27.0	2.13–26.37
Index range	$-40 \le h \le 21$	$20 \le h \le 19$
	$-23 \le k \le 23$	$0 \le k \le 13$
	$-50 \le l \le 50$	$0 \le l \le 25$
Reflections collected	76621	6948
Independent reflections	25733	6948
R_{int}	0.0619	0.0
Parameters	1497	505
GOF	0.901	0.960
R_1/wR_2 [$I > 2\sigma(I)$]	0.0539/0.1182	0.0298/0.0673
R_1/wR_2 (all data)	0.1001/0.1307	0.0403/0.0700
Extinction coefficient	0	0
Largest difference peak/hole [e Å^{-1}]	1.416/–0.607	0.936/–0.547

668223 (**4**), and -668222 (**6**) contain the supplementary crystallographic data for this paper. These data can be obtained free of charge from The Cambridge Crystallographic Data Centre via www.ccdc.cam.ac.uk/data_request/cif.

Cyclic Voltammetry: Measurements were performed in CH_2Cl_2 with 0.4 M [nBu$_4$N][ClO$_4$] as supporting electrolyte. An Amel 5000 system was used with a Pt wire as working electrode and a Pt plate (0.6 cm^2) as auxiliary electrode. The potentials were measured against Ag/AgPF$_6$ and were referenced against $E_{1/2}$(FcH/FcH$^+$) = 0 V.

NLO Measurements: For the second-order NLO measurements of the ionic chromophores, hyper-Rayleigh scattering[30] has been used to obtain the first hyperpolarizability. The measurements at a fundamental wavelength of 800 nm were performed in nitromethane, with crystal violet in methanol as the reference. The experimental setup and the data analysis have been described earlier.[32,33] The frequency-resolved approach ensures accurate hyperpolarizability values, not affected by multi-photon fluorescence.[32]

[1] M. Wagner, *Angew. Chem. Int. Ed.* **2006**, *45*, 5916–5918.
[2] G. Vives, A. Carella, S. Sistach, J.-P. Launay, G. Rapenne, *New J. Chem.* **2006**, *30*, 1429–1438.
[3] D. Astruc, *Electron Transfer and Radical Processes in Transition-Metal Chemistry*, Wiley-VCH, Weinheim, **1995**.
[4] D. Astruc, *Acc. Chem. Res.* **1997**, *30*, 383–391.
[5] B. Bildstein, *Coord. Chem. Rev.* **2000**, *206–207*, 369–394.
[6] S. Dabek, M. H. Prosenc, J. Heck, *J. Organomet. Chem.* **2007**, 2216–2226.
[7] J. J. Wolff, R. Wortmann, *Adv. Phys. Org. Chem.* **1999**, *32*, 121–217.
[8] M. P. Cifuentes, C. E. Powell, J. P. Morall, A. M. McDonagh, N. T. Lucas, M. G. Humphrey, M. Samoc, S. Houbrechts, I. Asselberghs, K. Clays, A. Persoons, T. Isoshima, *J. Am. Chem. Soc.* **2006**, *128*, 10819–10832; Z. Li, A. Qin, J. W. Y. Lam, Y. Dong, Y. Dong, C. Ye, I. D. Williams, B. Z. Tang, *Macromolecules* **2006**, *39*, 1436–1442.
[9] M. Iyoda, T. Kondo, T. Okabe, H. Matsuyama, S. Sasaki, Y. Kuwatani, *Chem. Lett.* **1997**, 35–36.
[10] P. Stepnicka, I. Cisarova, J. Sedlacek, J. Vohlidal, M. Polasek, *Collect. Czech. Chem. Commun.* **1997**, *62*, 1577–1584.
[11] S. Fiorentini, B. Floris, P. Galloni, F. Grepioni, M. Polito, P. Tagliatesta, *Eur. J. Org. Chem.* **2006**, 1726–1732.
[12] Y. Sasaki, C. U. Pittman Jr, *J. Org. Chem.* **1973**, *38*, 3723–3726.
[13] K. Schlögl, H. Soukup, *Monatsh. Chem.* **1968**, *99*, 927–946.
[14] H. K. Gupta, N. Reginato, F. O. Ogini, S. Brydges, M. J. McGlinchey, *Can. J. Chem.* **2002**, *80*, 1546–1554.
[15] H. Wong, T. Meyer-Friedrichsen, T. Farrell, C. Mecker, J. Heck, *Eur. J. Inorg. Chem.* **2000**, 631–646.
[16] T. Meyer-Friedrichsen, C. Mecker, M. H. Prosenc, J. Heck, *Eur. J. Inorg. Chem.* **2002**, 239–248.
[17] T. Meyer-Friedrichsen, H. Wong, M. H. Prosenc, J. Heck, *Eur. J. Inorg. Chem.* **2003**, 936–946.
[18] F. Rebiere, O. Samuel, H. B. Kagan, *Tetrahedron Lett.* **1990**, *31*, 3121–3124; U. T. Müller-Westerhoff, Z. Yuan, G. Ingram, *J. Organomet. Chem.* **1993**, *463*, 163–167.
[19] a) F. Grepioni, G. Cojazzi, D. Braga, E. Marseglia, L. Scaccianoce, B. F. G. Johnson, *J. Chem. Soc., Dalton Trans.* **1999**, 553–558; b) B. M. Trost, C. M. Older, *Organometallics* **2002**, *21*, 2544–2546.
[20] a) P. J. Fagan, M. D. Ward, J. C. Calabrese, *J. Am. Chem. Soc.* **1989**, *111*, 1698–1719; b) B. Steinmetz, W. A. Schenk, *Organometallics* **1999**, *18*, 943–946.
[21] J. D. Dunitz, *Acta Crystallogr., Sect. B* **1979**, *35*, 1068–1074.
[22] G. L. Hardgrove, D. H. Templeton, *Acta Crystallogr.* **1959**, *12*, 28–32.
[23] G. Meister, H. Stoeckli-Evans, G. Süss-Fink, *J. Organomet. Chem.* **1993**, *453*, 249–253.
[24] M. Rosenblum, in *Chemistry of the Iron Group Metallocenes*, Wiley Interscience, New York, **1965**, chapter 2.
[25] Y. S. Sohn, D. N. Hendrickson, H. B. Gray, *J. Am. Chem. Soc.* **1971**, *93*, 3603–3612.
[26] a) A. M. McNair, J. L. Schrenk, K. R. Mann, *Inorg. Chem.* **1984**, *23*, 2633–2640; b) J. K. Evju, K. R. Mann, *Organometallics* **2002**, *21*, 993–996.
[27] J. C. Calabrese, L.-T. Cheng, J. C. Green, S. R. Marder, W. Tam, *J. Am. Chem. Soc.* **1991**, *113*, 7227–7232.
[28] Y. Li, E. M. W. Tsang, A. Y. C. Chan, H.-Z. Yu, *Electrochem. Commun.* **2006**, *8*, 951–955.
[29] S. Barlow, D. O'Hare, *Chem. Rev.* **1997**, *97*, 637–669; J. M. Manriquez, M. D. Ward, J. C. Calabrese, P. J. Fagan, A. J. Epstein, J. S. Miller, *Mol. Cryst. Liq. Cryst.* **1989**, *126*, 527–534.
[30] a) K. Clays, A. Persoons, *Phys. Rev. Lett.* **1991**, *66*, 2980–2983; b) K. Clays, A. Persoons, *Rev. Sci. Instrum.* **1992**, *63*, 3285–3289.
[31] M. C. Flipse, R. de Jonge, R. H. Woudenberg, A. W. Marsman, C. A. van Walree, L. W. Jenneskens, *Chem. Phys. Lett.* **1995**, *245*, 297–303.
[32] O. F. J. Noordman, N. F. van Hulst, *Chem. Phys. Lett.* **1996**, *253*, 145–150.
[33] G. Olbrechts, R. Strobbe, K. Clays, A. Persoons, *Rev. Sci. Instrum.* **1998**, *69*, 2233–2241.
[34] J. L. Oudar, D. S. Chemla, *J. Chem. Phys* **1977**, *66*, 2664–2668.
[35] E. Hendrickx, K. Clays, A. Persoons, C. Dehu, J. L. Bredas, *J. Am. Chem. Soc.* **1995**, *117*, 3547–3555.
[36] U. Schöberl, T. F. Magnera, R. M. Harrison, F. Fleischer, J. L. Pflug, P. F. H. Schwab, X. Meng, D. Lipiak, C. Noll, V. S. Allured, T. Rudalevig, S. Lee, J. Michl, *J. Am. Chem. Soc.* **1997**, *119*, 3907–3917.
[37] K. Eichhorn, O. Treutler, H. Öhm, M. Häser, R. Ahlrichs, *Chem. Phys. Lett.* **1995**, *242*, 652–660.
[38] a) A. D. Becke, *J. Chem. Phys.* **1986**, *84*, 4524–4529; A. D. Becke, *J. Chem. Phys.* **1988**, *88*, 1053–1062; b) A. D. Becke, *Phys. Rev. A* **1988**, *38*, 3098–3100.
[39] J. P. Perdew, *Phys. Rev. B* **1986**, *33*, 8822–8824; J. P. Perdew, *Phys. Rev. B* **1986**, *34*, 7406.
[40] R. Ahlrichs, M. Bär, M. Häser, H. Horn, C. Kölmel, *Chem. Phys. Lett.* **1989**, *162*, 165–169.
[41] M. Häser, R. Ahlrichs, *J. Comput. Chem.* **1989**, *10*, 104–111.
[42] B. I. Dunlap, J. W. D. Connolly, J. R. Sabin, *J. Chem. Phys.* **1979**, *71*, 3396–4302.
[43] a) G. M. Sheldrick, *SHELXS-86, Program for Crystal Structure Determination*, University of Göttingen, Germany, **1986**; b) G. M. Sheldrick, *SHELXL-97, Program for Crystal Structure Refinement*, University of Göttingen, Germany, **1973**.

Received: November 26, 2007
Published Online: March 13, 2008

